Temperature-dependent phonon lifetimes in lead investigated with neutron-resonance spin-echo spectroscopy

K. Habicht,[1,2] R. Golub,[1] F. Mezei,[1] B. Keimer,[3] and T. Keller[3,4]
[1]*Hahn-Meitner-Institut, Glienicker Straße 100, D-14109 Berlin, Germany*
[2]*Technische Universität Darmstadt, Institut für Festkörperphysik, Hochschulstraße 6, D-64289 Darmstadt, Germany*
[3]*Max-Planck-Institute for Solid State Research, Heisenbergstraße 1, D-70569 Stuttgart, Germany*
[4]*FRM-II, Lichtenbergstraße 1, D-85747 Garching, Germany*
(Received 1 September 2003; published 22 March 2004)

An experimental study of phonon lifetimes in lead using a novel high-resolution neutron spectrometer is presented. The spectrometer combines the neutron-resonance spin-echo and the three-axis techniques. Transverse-acoustic phonon modes in the low-q limit along the high-symmetry directions are investigated at temperatures between 5–300 K. We apply an analytical approach based on a Gaussian approximation of the instrumental resolution function to separate intrinsic lifetimes from artifactual damping due to sample mosaicity and curvature of the four-dimensional dispersion surface. Observed linewidths are significantly lower than predicted by a theoretical model of anharmonic lattice dynamics based on a force-constant parametrization of the interatomic potential. In the high-symmetry directions the q dependence of the linewidth is found to be linear. No change in lifetime is observed at the superconducting transition temperature T_C.

DOI: 10.1103/PhysRevB.69.104301 PACS number(s): 78.70.Nx, 63.20.Kr, 63.20.Ry

I. INTRODUCTION

Phonons in elemental metals have first been studied in the early 1960s by Brockhouse[1] and Stedman[2] using three-axis neutron spectrometers. They obtained detailed phonon-dispersion relations, but intrinsic phonon linewidths arising from microscopic effects such as the electron-phonon and phonon-phonon scattering could only be resolved in a few favorable cases. The reason for this limited energy resolution is the limited neutron source flux, which was increased only by about one order of magnitude during the last four decades. Significant progress in spectrometer design and in the use of focusing components allows to reach very high resolution in favorable cases.[3] But in general even at modern high-flux neutron-sources the standard inelastic neutron-scattering techniques are restricted to energy resolutions in the meV range, introducing large errors in the accuracy of phonon linewidth measurements. Experiments using Raman scattering reach resolution in the μeV range and can resolve intrinsic phonon linewidths, but are restricted to optical modes at the Brillouin-zone center. For lead, the latest neutron study dates back to 1970.[4] Due to the lack of new experimental data, there is also only limited theoretical work,[5–8] although modern theoretical methods and *ab initio* calculations should be able to predict phonon energies and linewidths for each phonon branch.[9,10]

Novel neutron spectrometers combining the neutron spin-echo[11] (NSE) and three-axis spectrometry (TAS) techniques allow us to measure linewidths of *dispersing* excitations, including both phonons and magnons. NSE allows to increase the energy resolution by several orders of magnitude without excessive loss of intensity. The basic idea of NSE is to use differences of the Larmor precession phase of an initially polarized neutron beam running through uniform magnetic fields (precession fields) before and after the sample to encode the energy transfer. Mezei[12] and Pynn[13] pointed out that the spin-echo resolution function can be tuned to the slope of the dispersion curve (group velocity) by tilting the boundaries of the precession fields relative to the neutron beam.

Considerable effort was undertaken to implement inclined field boundaries on conventional NSE spectrometers with dc precession coils, but problems with stray fields at the coil boundaries impeded essential progress. In a first approach in the early 1980s Zeyen[14] used compact iron frame electromagnets with vertical dc fields. The coils worked well for quasielastic scattering and for the measurement of phonon excitations on dispersionless branches[15–18] with field boundaries perpendicular to the neutron beam (zero tilt angle). However severe problems were reported for nonzero tilt angles.

Mezei followed a different approach: instead of rotating the main precession coils, he added special gradient coils to the main solenoids of the NSE instrument IN11 at ILL, Grenoble[19] generating a field gradient in the horizontal direction perpendicular to the neutron beam. This way effective tilt angles in the order of 10° were obtained, which allowed the measurement of phonon linewidths in superfluid ^{4}He.[20] Those phonons had relatively small group velocities ($v_g \simeq 200$ m/s), i.e., one order of magnitude smaller than typical acoustic phonons in solids. The gradient coil technique was later also used by Zeyen[21] on the thermal three-axis instrument IN20 at ILL and by Zeyen and Kakurai[22] at the three-axis spectrometer PONTA at JAERI (Japan), but to date only quasielastic experiments were reported from these instruments.

A new solution became available with the NRSE (neutron-resonance spin-echo) technique introduced by Golub and Gähler.[23] This technique uses small radio frequency (rf) spin flippers instead of large dc coils to define the precession regions (Fig. 1). The field boundaries are geometrically defined by the precise windings of the rf flippers.

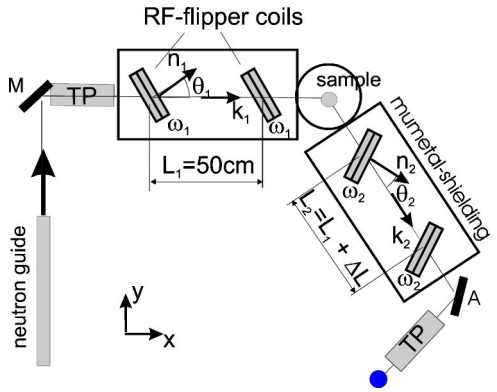

FIG. 1. Experimental setup of the NRSE spectrometer at BENSC, Berlin. M, monochromator (pyrolytic graphite PG, vertically focusing); A, analyzer (PG, flat); TP, supermirror transmission polarizer and analyzer. The rf-flipper coils and the sample are housed inside a mu-metal magnetic shield (shielding factor 100). Each rf-flipper coil can be rotated around a vertical axis (z). $\mathbf{n}_{1,2}$ are normal vectors to the coil surfaces, $\theta_{1,2}$ are the coil inclination angles, $\mathbf{k}_{1,2}$ are the neutron wave vectors. The last coil in front of the analyzer (A) can be translated along the beam direction to tune the length L_2 of the second arm.

Along the flight path between the rf flippers no magnetic field is applied. A special setup using pairs of identical rf flippers with opposite dc fields (*bootstrap* technique[24]) reduces stray fields to negligible values. Large field tilt angles up to 50° are easily obtained by rotating the rf flippers about a vertical axis.

The results presented in this paper were obtained from a new spectrometer incorporating the combined NRSE-TAS technique. This instrument was developed at the Technical University Munich and installed at the TAS V2 at BENSC (Berlin Neutron Scattering Center).[25–27] The instrument suffers from two restrictions: First it is located at a neutron guide at the cold neutron source, which restricts the incident neutron energy and thus the excitation energy to values <5 meV. Second the neutron flux at Berlin Neutron Scattering Center (BENSC) is about one order of magnitude lower than at leading high-flux sources, thus restricting experiments to large crystals. Presently two NRSE-TAS instruments avoiding these limitations are under construction at the new high-flux source FRM-II, Munich[28] and at the ILL, Grenoble.[29]

The maximum energy resolution of a NRSE-TAS spectrometer is given by the maximum radio frequency applied to the rf spin-flip coils. Instrumental resolution effects originating from finite beam collimation and monochromaticity and from sample properties, e.g., mosaicity and curvature of the dispersion surface, lead to artifactual line broadening effects. Quantitative knowledge of the instrumental resolution and of the influence of sample properties is a necessary prerequisite to extract intrinsic lifetimes from experimental data. In this work we apply an analytical approach[30] which allows us to correct the data for these extraneous effects.

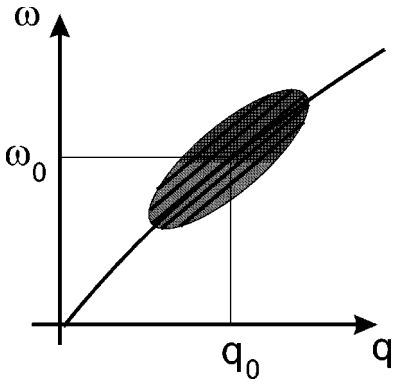

FIG. 2. The resolution function of the *host* three-axis spectrometer (ellipsoid) selects a region in the $(\mathbf{q},\omega)$ space. High-ω resolution is provided by the NRSE spectrometer. The lines $\phi_{NSE}=$const have to be oriented parallel to the dispersion curve (spin-echo phonon focusing) by inclining the precession field boundaries.

II. BASIC PRINCIPLES OF SPIN-ECHO PHONON FOCUSING

For conventional NSE instruments with precession field boundaries perpendicular to the neutron beam path the spin-echo phase $\phi_{NSE}(\omega)=\phi_2-\phi_1$ is proportional to the energy transfer ω and independent of the momentum transfer $\hbar\mathbf{Q}$. $\phi_{1,2}$ are the Larmor phases accumulated in the first (second) spectrometer arm. In the case of quasielastic scattering processes, where the mean excitation energy is zero and thus independent of $\mathbf{Q}$, one can use an incoming beam with broad spectral distribution (typically $\Delta\lambda/\lambda=10\%$) and thus a very relaxed $\mathbf{Q}$ resolution without losing energy resolution. In the case of dispersive excitations such as phonons, where the energy transfer ω depends on the wave vector of the excitation $\mathbf{q}$, $\omega=\omega(\mathbf{q})$, a finite momentum resolution leads to a spread in ω and in $\phi_{NSE}(\omega)$ even for an excitation with zero linewidth. To be able to measure the intrinsic linewidths of phonons, the spin-echo phase has to be tuned to the slope (group velocity) $\mathbf{v}_g=\boldsymbol{\nabla}_\mathbf{q}\omega$ of the dispersion surface to get constant $\phi_{NSE}(\omega,\mathbf{q})$ for all scattering events lying on a line with slope $\mathbf{v}_g$ (Fig. 2).

It was pointed out by Mezei[12] that such a first-order focusing can be achieved by inclining the boundaries of the precession fields relative to the beam path. In this case all neutrons scattered from an excitation with zero linewidth and a linear dispersion have the same spin-echo phase ϕ_{NSE}, a finite linewidth causes a spread in ϕ_{NSE}, which leads to a beam polarization proportional to the Fourier transform of the spectral line shape.

For a phonon with energy ω_0, momentum $\mathbf{q}_0$, and group velocity $\boldsymbol{\nabla}_q\omega(\mathbf{q}_0)$, we require the Larmor precession phase after the second coil to be a linear function:

$$\Delta\phi_{NSE}=\phi_{NSE}-\underline{\phi}_{NSE}=\tau_{NSE}\Delta\omega, \tag{1}$$

where

$$\Delta\omega=\omega-\omega_0(\mathbf{q})=\omega-[\omega_0(\mathbf{q}_0)+(\mathbf{q}-\mathbf{q}_0)\cdot\nabla_q\omega(\mathbf{q}_0)]$$

with $\phi_{NSE}=\phi_{NSE}(\mathbf{q}_{0,}\omega_0)$. $(\mathbf{q}_{0,}\omega_0)$ are the nominal phonon wave vector and energy (Fig. 2). τ_{NSE} is called *spin-echo time*.

Mezei has shown that in order to satisfy Eq. (1) the normal vectors to the coil surfaces have to be oriented such that

$$\mathbf{n}_{1,2}\| \left(\underline{\mathbf{k}}_{1,2} - \frac{m}{\hbar} \nabla_q \omega_o \right) \tag{2}$$

or

$$\cos\theta_{1,2} = \frac{\underline{\mathbf{k}}_{1,2} \cdot \left(\underline{\mathbf{k}}_{1,2} - \frac{m}{\hbar} \nabla_q \omega_o \right)}{\underline{k}_{1,2} \left| \underline{\mathbf{k}}_{1,2} - \frac{m}{\hbar} \nabla_q \omega_o \right|}. \tag{3}$$

The index 1 (2) refers to the first (second) spectrometer arm. $\mathbf{k}_{1,2}$ are the mean neutron wave vectors. The rf $\omega_{1,2}$ applied to the coils in the first and the second arm have to be adjusted to the ratio

$$\frac{\omega_1 L_1}{\omega_2 L_2} = \frac{k_1^3 \left(\mathbf{1} - \frac{m}{\hbar} \underline{\mathbf{k}}_1 \cdot \nabla_q \omega_o / k_1^2 \right)}{k_2^3 \left(\mathbf{1} - \frac{m}{\hbar} \underline{\mathbf{k}}_2 \cdot \nabla_q \omega_o / k_2^2 \right)}. \tag{4}$$

If these tuning conditions, Eqs. (2) and (4) are satisfied, we get

$$\tau_{NSE} = \left(\frac{m}{\hbar} \right)^2 \frac{\omega_{1,2} L_{1,2}}{\underline{k}_{1,2}^3} \frac{1}{\left(\mathbf{1} - \frac{m}{\hbar} \underline{\mathbf{k}}_{1,2} \cdot \nabla_q \omega_o / k_{1,2}^2 \right)}, \tag{5}$$

where τ_{NSE} is the same for the first and the second spectrometer arm (indices 1 and 2).

Neglecting instrumental effects and the $\mathbf{Q}$ dependence of the scattering function $S(\mathbf{Q},\omega)$, the polarization of the scattered beam at the exit of the second spectrometer arm is given by

$$P(\tau_{NSE}) \propto \int S(\omega) \cos(\omega \tau_{\mathrm{NSE}}) d\omega, \tag{6}$$

i.e., the Fourier transform of the scattering function $S(\omega)$. Thus a Lorentzian with half width at half maximum Γ,

$$S(\omega) = \frac{1}{\pi} \frac{\Gamma}{\Gamma^2 + \omega^2},$$

transforms to an exponential decay of the polarization:

$$P(\tau_{\mathrm{NSE}}) = \exp(-\Gamma \tau_{\mathrm{NSE}}). \tag{7}$$

The influence of resolution effects on $P(\tau_{\mathrm{NSE}})$ is discussed in Sec. IV.

III. EXPERIMENT

Inelastic neutron-scattering experiments were conducted at the cold three-axis spectrometer V2 (FLEX) at the BENSC. This instrument can optionally be equipped with an NRSE setup.[31]

Two different high-quality Pb single crystals have been used in the experiments. These cylindrical shaped crystals had 30 mm diameter and 40 mm height and have been mounted in a standard Orange cryostat with their cylinder axes (110) or (100) perpendicular to the scattering plane.

In order to satisfy the spin-echo conditions [Eqs. (2) and (4)] the phonon energy $\hbar\omega_0$ and the slope of the dispersion curves $\nabla_q \omega_0(\mathbf{q}_0)$ at the phonon wave vector $\mathbf{q}_0$ have to be known. These quantities have been obtained from a Born–von Kàrmàn fit to dispersion data from the literature.[1,4] Where measurements at temperatures different than the dispersion data of the above cited literature have been performed, $\hbar\omega_0$ and $\nabla_q \omega_0(\mathbf{q}_0)$ were interpolated.

The spectrometer was configured in the SM$=-1$, SS$=-1$, SA$=+1$ scattering senses with fixed $k_1=1.7$ Å^{-1} (SM, SS, SA: scattering sense at monochromator, sample, analyzer; -1, clockwise). The monochromator (PG 002) was used vertically focusing with a curvature $\rho_M=0.3$ m^{-1} and a tunable PG filter[32] was installed to suppress second-order contamination. Two supermirror ($m\simeq 2$) transmission-type polarizers were used, installed after the monochromator and after the flat PG analyzer. No additional collimators were used.

To measure the phonon lifetimes for a particular phonon mode and temperature the TAS was set to the nominal $\mathbf{Q}$, E values where it was kept fixed during spin-echo scans. Measurements were always performed at $k_2<k_1$. The spin-echo focusing conditions then require the TAS to be configured in a TAS-defocused mode. A TAS-focused mode would result in large coil tilt angles ($|\theta|>50°$), which are experimentally inaccessible. The configuration used in our experiments offers high-Q resolution in the direction parallel to $\mathbf{q}_0$. Typically a transverse Q resolution of about 0.015 Å^{-1} FWHM (full width at half maximum) was achieved. The tilt angles $\theta_{1,2}$ and the frequency ratio ω_1/ω_2 were set according to the calculated values. Typical values were $\theta_1=-30°$ and $\theta_2=+25°$ for $[\xi 00]$ transverse-acoustic (TA) phonons with $\xi<0.2$ r.l.u.

Due to the relatively large observed linewidths Γ, the range of the spin-echo time τ_{NSE} used for the spin-echo measurements was typically between 10 and 50 ps. For τ_{NSE} above this range the polarization P [Eq. (7)] usually decayed to zero. The technical limits of the spin-echo time for the spectrometer as used in the configuration for this experiment are 10 ps$\lesssim\tau_{\mathrm{NSE}}\lesssim$300 ps.

To measure the polarization for a given τ_{NSE}, the field integral $\omega_2 L_2$ of the second spectrometer arm is varied by translating the last rf coil through a small distance ΔL. This causes the intensity to oscillate,

$$I(\Delta L) = I_0\{1 + P\cos[2\pi(\Delta L + \Delta L_0)/\Delta L_p]\}, \tag{8}$$

where $\Delta L_P = 2\pi\hbar k_2/(m_n\omega_2)$ is the oscillation period, ΔL_0 is an offset, I_0 is the average intensity. These ΔL scans run through one period ΔL_P (see Fig. 3), typically a few millimeters. The polarization P is extracted by fitting Eq. (8), where the period ΔL_P is known from the instrumental pa-

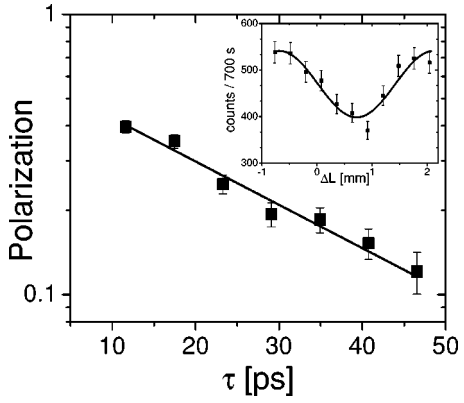

FIG. 3. Polarization as a function of spin-echo time τ for the [2 0.1 0] phonon, $T=200$ K. In the semilogarithmic plot the exponential decay of the polarization shows up as a straight line. Inset: Spin-echo ΔL scan at $\tau=40.7$ ps.

rameters. The polarization is determined for at least four different values of τ_{NSE} per phonon and temperature by changing the rf, however keeping the ratio ω_1/ω_2 fixed.

IV. DATA CORRECTION

The linewidth data as obtained from our measurements (see Table I) represent an upper limit on the intrinsic linewidth (lower limit on the intrinsic lifetime). We now discuss different instrumental sources of signal depolarization that mask the intrinsic line broadening: (i) depolarization due to field inhomogeneities and stray fields of the rf spin-flip coils, (ii) instrumental resolution effects, due to the fact that the Larmor phase depends in second order on the beam monochromaticity and divergence, (iii) instrumental misalignment due to inaccurate dispersion data, (iv) sample mosaicity, and (v) influence of the curvature of the dispersion surface.

(i) Stray fields are excluded as a significant source of signal depolarization from calibration measurements. This was verified by measuring the polarization as a function of frequency and coil tilt angles in the unscattered beam.

(ii) Instrumental resolution effects resulting from beam monochromaticity and divergence cannot reach a significant level in the τ range covered by our experiments. This has been shown by calculating the polarization as a function of τ. In the general case the polarization of the scattered beam obtained by a combination of a spin-echo and a three-axis instrument is proportional to

$$P \propto \int S(\mathbf{Q},\omega) T(\mathbf{k}_1,\mathbf{k}_2) e^{i\phi(\tau,\mathbf{k}_1,\mathbf{k}_2)} d^3k_1 d^3k_2 + \text{c.c.}, \quad (9)$$

where $S(\mathbf{Q},\omega)$ is the scattering function, $T(\mathbf{k}_1,\mathbf{k}_2)$ is the TAS transmission probability, and $\phi(\tau,\mathbf{k}_1,\mathbf{k}_2)$ is the difference of the Larmor precession angles in the first and the second arm. Equation (9) has been evaluated based on the following assumptions: (1) The TAS transmission probability is adequately described by a Gaussian approximation based on the Cooper and Nathans approach;[33] (2) the remaining **Q** dependence in the Larmor phase can be treated by a second-order expansion of the total Larmor angle; (3) the intrinsic linewidth is assumed to vanish. Numerical data of the depolarization as a function of spin-echo time τ are shown in Fig. 4.

(iii) Instrumental misalignment errors have been discussed in detail by Pynn.[13] These can be ruled out as a significant source of signal depolarization in our lifetime mea-

TABLE I. Experimental phonon linewidth data. Phonon modes $[\xi\xi\xi]$ are given in r.l.u. Data in the (011) direction refer to the T_1 branch. Temperatures T are given in kelvin. Phonon energies E are given in meV. Γ (μeV) is the half width at half maximum (HWHM) as obtained from the experimental data. Γ_{CM} (μeV) is the HWHM after correcting for curvature of the dispersion surface and sample mosaic spread.

$[\xi\xi\xi]$	T	E	Γ	Γ_{CM}
0.025 0.025 0.025	300	0.315	26(2)	14(2)
	100	0.343	20(2)	8(2)
	50	0.350	26(3)	12(3)
0.05 0.05 0.05	300	0.627	29(1)	21(1)
	100	0.681	11(3)	2(3)
0.1 0.1 0.1	300	1.228	43(7)	40(7)
	200	1.280	36(6)	32(6)
	100	1.332	33(5)	28(5)
0 0.025 0.025	300	0.364	26(2)	6(2)
	50	0.391	23(1)	1(1)
	10	0.395	20(3)	−3(3)
	5	0.396	22(3)	0(3)
0 0.05 0.05	300	0.724	31(3)	15(3)
	200	0.744	26(2)	10(2)
	100	0.767	22(2)	6(2)
	50	0.778	19(2)	3(2)
	15	0.786	18(4)	2(4)
	5	0.788	17(3)	1(3)
0 0.1 0.1	300	1.411	46(8)	38(8)
	200	1.461	25(3)	16(3)
	100	1.515	24(3)	14(3)
	50	1.543	19(3)	9(3)
0 0.15 0.15	300	2.088	20(9)	14(9)
0 0 0.05	300	0.439	23(1)	7(1)
	10	0.559	15(6)	−5(6)
0 0 0.1	300	0.879	28(2)	18(2)
	200	0.952	24(2)	13(2)
	100	1.040	25(2)	13(2)
	50	1.084	17(3)	4(3)
	10	1.119	15(2)	1(2)
	5	1.124	14(3)	0(3)
0 0 0.15	300	1.318	34(2)	26(2)
	200	1.422	31(3)	23(3)
	150	1.480	24(2)	15(2)
	100	1.537	22(3)	12(3)
	50	1.595	13(4)	3(4)
0 0 0.2	300	1.757	51(7)	45(7)
	200	1.881	45(7)	39(7)
	100	2.019	29(4)	22(4)

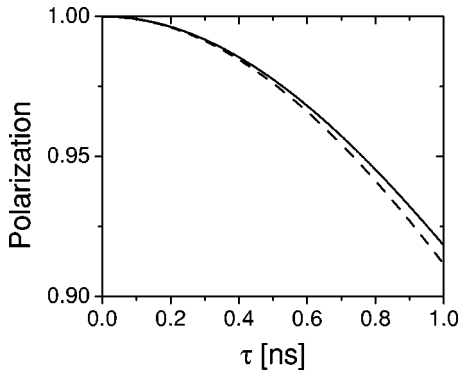

FIG. 4. Depolarization due to purely instrumentally limited resolution, assuming $\Gamma=0$, perfect sample (no mosaic spread, planar, i.e., uncurved dispersion) as calculated for the [2 0.1 0] TA phonon. Scattering senses are at the monochromator SM$=-1$, at the sample SS$=-1$, and at the analyzer SA$=+1$ (solid curve) or SA$=-1$ (dashed curve). Note that the τ range of our spectrometer is restricted to $\tau<0.3$ ns. The present experiments were performed up to $\tau\approx 50$ ps.

surements. In particular we investigated the polarization behavior as a function of frequency or tilt-angle detuning (Fig. 5).

Since the instrument parameters are calculated from the dispersion data, incorrect values for the excitation energy and group velocity lead to wrong coil tilt angle and frequency settings. To estimate the effect of false dispersion data we have calculated the depolarization assuming a 10% error in both the nominal phonon energy $\hbar\omega_0$ and the slope

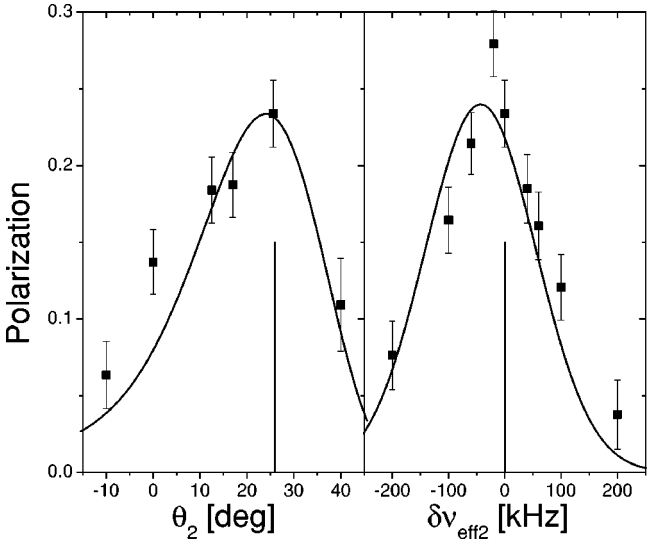

FIG. 5. Detuning of phonon-focusing parameters for the [2 0.1 0] TA phonon at at $\tau=35$ ps, $T=150$ K. Left: Tilt-angle detuning in the second arm. Right: Frequency detuning in the second arm. Solid lines result from a resolution calculation (Ref. 30). Nominal parameters are indicated by vertical bars. As the coil tilt angles are controlled with an accuracy of 0.01° and the frequencies are derived from a quartz oscillator, we conclude that in our τ range depolarization due to instrumental misalignment is below the statistical error.

$\nabla_q\omega_0(\mathbf{q}_0)$ of the dispersion curves. Since we are in the linear regime of the dispersion, we have assumed that the *relative* errors in phonon energy and slope of the dispersion are the same. Assuming an intrinsic linewidth of $\Gamma_{intr}=20.00$ μeV would correspond to an experimental linewidth $\Gamma_{expt}=20.62$ μeV if we assume $+10\%$ error in $\hbar\omega_0$ and $\nabla_q\omega_0(\mathbf{q}_0)$. For a -10% error $\Gamma_{expt}=19.85$ μeV is obtained. The difference in absolute errors is due to the asymmetry of the polarization with respect to the nominal values as is also seen in Fig. 5. We conclude that rather coarse knowledge of the dispersion data on a 10% accuracy level, as is easily obtained from standard TAS scans, is sufficient for linewidths $\Gamma\gtrsim 20$ μeV ($\tau<200$ ps). For linewidths in the μeV range ($\tau>200$ ps) the dispersion input parameters would have to be known with higher accuracy.

(iv) Taking sample mosaic into account and assuming a Gaussian mosaic distribution the polarization will be reduced by a factor[30]

$$\sqrt{2\pi\eta_\Sigma}\,e^{-(1/2)\tau^2|\nabla_q\omega_0(\mathbf{q}_0)|^2|\mathbf{G}_0|^2\sin^2\vartheta\,\eta_\Sigma^2}, \tag{10}$$

i.e., a Gaussian with 1σ standard deviation $(|\nabla_q\omega_0(\mathbf{q}_0)||\mathbf{G}_0|\sin\vartheta\eta_\Sigma)^{-2}$. Here η_Σ denotes the mosaicity expressed as 1σ standard deviation. ϑ is the angle between the mean reciprocal-lattice vector $\mathbf{G}_0$ and the phonon wave vector $\mathbf{q}_0$.

The mosaicity η of our crystals was measured using a novel spin-echo diffraction technique (Larmor diffraction[34]) with the same NRSE setup as was used for the linewidth measurements. The advantage of this Larmor diffraction technique is that the same beam size can be used as for the linewidth determination. Thus we obtain the mosaicity for the same sample volume as is illuminated in the inelastic measurements. Using the (200) Bragg reflection and the same k_1 as for the inelastic measurements we obtained $\eta=(5.68\pm0.04)'$ FWHM and $\eta=(4.16\pm0.04)'$ FWHM for the two different crystals used in the experiments. For the [2 0.1 0] TA phonon in Pb the polarization is reduced by a factor of 2 at $\tau\approx 56$ ps (76 ps) for $\eta_S=5.7$ $'(4.2')$ FWHM. This significant effect has been included in the correction of our experimental lifetime data.

(v) The curvature of the dispersion surface is taken into account via the second-order derivative in the expansion of the dispersion relation. The spin-echo phase ϕ then has an additive term

$$-\tfrac{1}{2}\tau\Delta\mathbf{q}^T\hat{H}\Delta\mathbf{q}. \tag{11}$$

Here $\hat{H}$ is the symmetric (3×3) Hessian evaluated at the nominal wave vector $\mathbf{q}_0$,

$$H_{i,j}=\frac{\partial^2\omega}{\partial q_i\partial q_j},\quad i,j=1,2,3. \tag{12}$$

Since the curvature term is of second order, a correct description of curvature depolarization must include all possible second-order terms in the spin-echo phase. Horizontal and vertical resolution are then no longer decoupled. We have expanded the spin-echo phase up to second order and subsequently integrated Eq. (9) analytically. The following as-

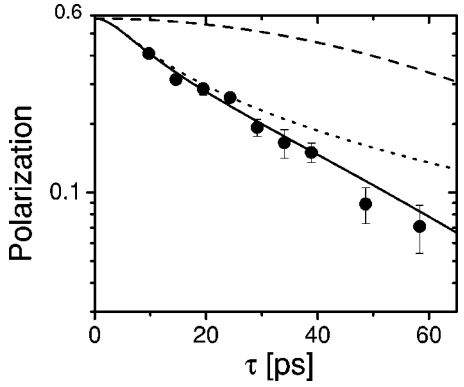

FIG. 6. Calculated depolarization due to sample mosaic (dashed), curvature (dotted), and both effects (solid). The calculated curves have been multiplied by a factor $P_0=0.58$ for a direct comparison with the experimental data. Experiment and theory refer to the [2 0.025 0.025] TA mode at $T=50$ K.

sumptions were made: (1) the spin-echo conditions are satisfied; (2) the sample is perfect (no mosaic spread); (3) the TAS transmission probability is adequately described by a Gaussian approximation based on the Cooper and Nathans approach; (4) the intrinsic linewidth is assumed to vanish; (5) the dispersion is approximated by a sinusoidal function. This model is adequate for the small q values investigated in the present experiment.

In addition to the instrumental spin-echo parameters the usual TAS parameters enter the resolution calculation. The monochromator and analyzer mosaic spreads are assumed to be $\eta_{M,A}=30'$, close to the experimental values.[35] Collimation parameters which describe the TAS resolution function are inferred from the effective collimation of the beam optical elements used in our setup. In the elastic limit the calculated TAS resolution function was experimentally checked by measuring the Bragg widths. At the (200) Bragg peak we obtain experimental (calculated) values: longitudinal Q resolution: $\Delta Q_x=0.014$ (0.014) Å^{-1}, transverse Q resolution $\Delta Q_y=0.014$ (0.011) Å^{-1}, and elastic energy resolution $\Delta E=0.071$ (0.071) meV. The evident agreement between calculated and measured values gives us confidence into our parametrization of the resolution function.

To correct for both, sample mosaic and curvature, the experimental polarization data have been normalized with the calculated data. The combined effect of mosaic and curvature is obtained by the product of the Gaussian, Eq. (10), and the integrated Eq. (9) including curvature terms.

At very low wave vectors q (as shown in Fig. 6) the intrinsic linewidth Γ is expected to vanish and the signal depolarization results from resolution effects only. The calculated resolution curve is in good agreement with the experimental data. For larger wave vectors q the intrinsic linewidth increases and the effect of the curvature decreases with increasing q (Fig. 7).

V. EXPERIMENTAL RESULTS

Within statistical error all measured phonon linewidths were in agreement with a single exponential decay [straight line $P(\tau)$ in a semilogarithmic plot, Fig. 3]. Thus we find no evidence for possible deviations from Lorentzian line shapes $S(\omega)$ predicted by theory at least for longitudinal modes.[36] The multiphonon background does not contribute significantly to our data.

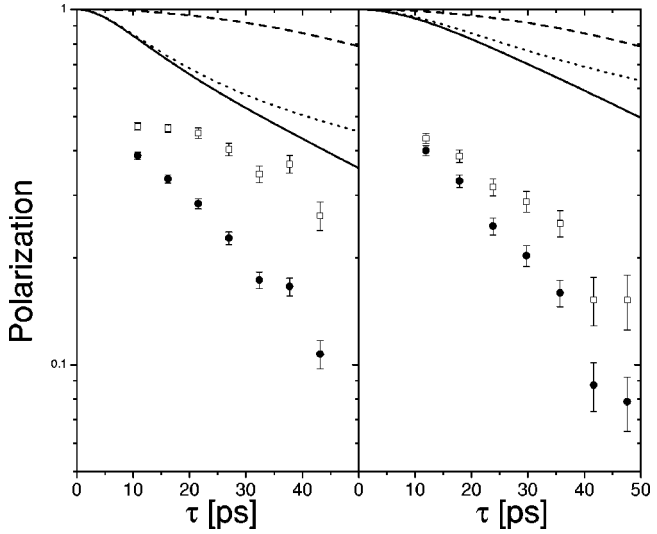

FIG. 7. Calculated depolarization due to sample mosaic (dotted), curvature (dashed), and a combination (solid) together with the experimental data (full circles) and normalized data (open squares). Left, [2 0.05 0] TA phonon; right, [2 0.1 0] TA phonon at $T=300$ K.

Linewidths Γ as obtained from the raw data and corrected linewidths Γ_{CM} are given in Table I and in Figs. 8–11.

Both temperature and wave-vector dependence of the intrinsic anharmonic linewidth of transverse-acoustic phonons have been determined at $q\neq 0$. The variation of the intrinsic linewidth with temperature or wave vector is well outside the error bars. The resolution obtained in the present experiment is at least one order of magnitude improved compared to earlier inelastic neutron-scattering data.[2,4] The statistical accuracy of the data is insufficient to detect a phonon linewidth anomaly at the superconducting transition temperature T_C.

VI. DISCUSSION

Single crystalline Pb is a representative of the structurally simple fcc metals where at high enough temperatures (T

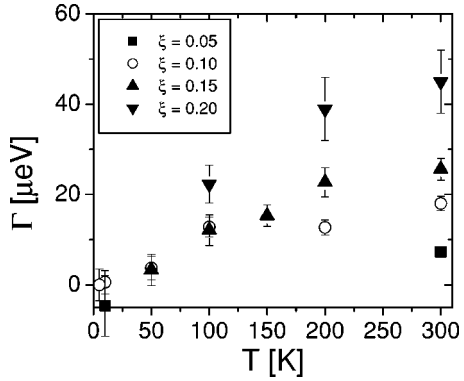

FIG. 8. Temperature dependence of the [ξ00] phonon linewidth Γ. ξ is given in r.l.u.

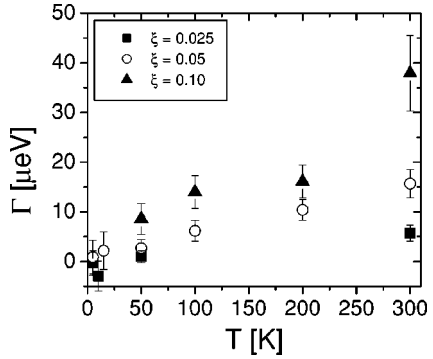

FIG. 9. Temperature dependence of the $[\xi\xi 0]$ T_1 phonon linewidth Γ. ξ is given in r.l.u.

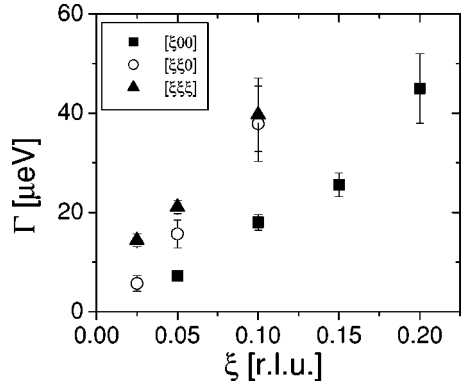

FIG. 11. ξ dependence of the phonon linewidth Γ at $T=300$ K.

>10 K) phonon-phonon interaction dominates over electron-phonon interaction and therefore can be regarded as a model system where phonon-phonon interaction can be studied by itself. *Ab-initio* calculations[37] show that the electron-phonon contribution to the phonon linewidths is negligible, thus supporting the hypothesis that the intrinsic linewidths extracted are due to phonon-phonon interaction. Furthermore due to the low Debye temperature $\theta_D \simeq 100$ K anharmonic effects become apparent in a wide range of temperatures conveniently accessible by experiment. The variation of the linewidth with temperature is clearly observed in our experiments.

For the simple fcc metals the lattice-dynamical problem was solved by using a force-constant parametrization of the interatomic potential.[8] This approach has also been applied to calculate linewidths for phonon modes in lead,[7] but a comparison between theory and experiment has been impeded due to the fact that two contradictory sets of experimental data for Pb phonon linewidths exist in the literature.[2,4] Zoli[7] obtains in general larger values for the linewidth than experimentally observed, e.g., $\Gamma=90$ μeV for the [0.1 0 0] TA mode in contrast to our data and the data of Furrer.[4] In the theoretical model harmonic constants are obtained from a fit to experimental phonon-dispersion data and macroscopic elastic constants. Anharmonic constants are obtained from a fit to the linear coefficient of thermal expansion and the thermodynamic Grüneisen parameter. The fact that the interatomic potential in the fcc metals is of long range implies a large number of parameters. Furthermore an approach with only central, two-body forces is not possible since the elastic constants do not satisfy the second-order Cauchy relations. In total the model relies on 22 harmonic force-constant parameters and four anharmonic force-constant parameters. The accuracy of the anharmonic parameters obtained from this non-*ab-initio* model is not quantified so that the accuracy of the theoretical prediction remains questionable.

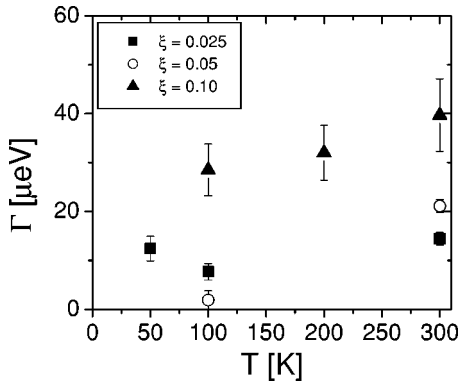

FIG. 10. Temperature dependence of the $[\xi\xi\xi]$ phonon linewidth Γ. ξ is given in r.l.u.

From our experiment the q dependence of the linewidth is found to be linear. Within statistical error no lifetime change at the superconducting transition is found for low-q phonons in the [110] and [100] directions, indicating that even at $T<10$ K the electron-phonon interaction plays no dominant role. This is in agreement with earlier inelastic neutron-scattering experiments by Youngblood *et al.*[38] on a TAS with instrumental resolution on the order of 100–200 μeV and contradicts the results of Bobrovskii *et al.*[39]

VII. CONCLUSIONS

The combined NRSE-TAS technique has been successfully applied to dispersive phonon modes. In single crystalline Pb broadening of the one-phonon peaks due to lattice anharmonicity resulting in Lorentzian linewidths could be measured with high accuracy. The resolution is improved by one order of magnitude as compared to conventional inelastic neutron spectroscopy. Intrinsic phonon linewidths were extracted by taking mosaicity and curvature of the dispersion explicitly into account with a resolution approach based on the Gaussian approximation of the TAS transmission function. The present data go quantitatively beyond previous inelastic neutron-scattering work and offer an opportunity to compare theoretical *ab initio* models with experiment.

ACKNOWLEDGMENTS

We thank Dr. R. Gähler and Professor W. Gläser for continuous support. Valuable discussions with Professor R. Pynn and Dr. P. Vorderwisch are gratefully acknowledged. We thank Dr. Ch. Lin for the growth of one of the Pb crystals used and B. Urban for technical assistance in the course of experiments.

[1] B.N. Brockhouse, T.A. Arase, G. Caglioti, K.R. Rao, and A.D.B. Woods, Phys. Rev. **128**, 1099 (1962).
[2] R. Stedman and G. Nilsson, Phys. Rev. **145**, 492 (1966).
[3] A. Göbel, D.T. Wang, M. Cardona, L. Pintschovius, W. Reichardt, J. Kulda, N.M. Pyka, K. Itoh, and E.E. Haller, Phys. Rev. B **58**, 10 510 (1998).
[4] A. Furrer and W. Hälg, Phys. Status Solidi **42**, 821 (1970).
[5] L. van Hove, Phys. Rev. **95**, 249 (1954).
[6] A.A. Maradudin and A.E. Fein, Phys. Rev. **128**, 2589 (1962).
[7] M. Zoli, J. Phys.: Condens. Matter **3**, 6249 (1991).
[8] M. Zoli, G. Santoro, V. Bortolani, A.A. Maradudin, and R.F. Wallis, Phys. Rev. B **41**, 7507 (1990).
[9] S.Y. Savrasov and D.Y. Savrasov, Phys. Rev. B **54**, 16 487 (1996).
[10] G. Lang, K. Karch, M. Schmitt, P. Pavone, A.P. Mayer, R.K. Wehner, and D. Strauch, Phys. Rev. B **59**, 6182 (1999).
[11] F. Mezei, Z. Phys. **255**, 146 (1972).
[12] F. Mezei, *Inelastic Neutron Scattering* (IAEA, Vienna, 1978), p. 125.
[13] R. Pynn, J. Phys. E **11**, 1133 (1978).
[14] C.M.E. Zeyen, in *Neutron Scattering–1981*, edited by John Faber, AIP Conf. Proc. No. 89 (AIP, New York, 1982), p. 101.
[15] E. Farhi, B. Fåk, C.M.E. Zeyen, and J. Kulda, Physica B **297**, 32 (2001).
[16] J. Kulda, E. Farhi, and C.M.E. Zeyen, Physica B **297**, 37 (2001).
[17] J. Kulda, E. Farhi, and C.M.E. Zeyen, Physica B **316-317**, 383 (2002).
[18] J. Kulda, A. Debernardi, M. Cardona, F. de Geuser, and E.E. Haller, Phys. Rev. B **69**, 045209 (2004).
[19] Institut Laue Langevin *Yellow Book*, see www.ill.fr
[20] F. Mezei, B. Farago, and C. Lartigue, in *Excitations in Two-Dimensional and Three-Dimensional Quantum Fluids*, Vol. 257 of *NATO Advanced Studies Institute, Series B: Physics*, edited by A.F.G. Wyatt and H.J. Lauter (Plenum, New York, 1991), p. 119.
[21] C.M.E. Zeyen, J. Phys. Chem. Solids **60**, 1573 (1999).
[22] C.M.E. Zeyen, K. Kakurai, N. Nishi, N. Nakajima, T. Sakaguchi, Y. Kawamura, S. Watanabe, M. Berneron, K. Sasaki, and Y. Endoh, Neutron News **8**, 7 (1997).
[23] R. Golub and R. Gähler, Phys. Lett. A **123**, 43 (1987).
[24] R. Gähler and R. Golub, J. Phys. (Paris) **49**, 1195 (1988).
[25] T. Keller, R. Golub, F. Mezei, and R. Gähler, Physica B **234**, 1126 (1997).
[26] T. Keller, R. Golub, F. Mezei and R. Gähler, Physica B **241-243**, 101 (1997).
[27] T. Keller, R. Golub, and R. Gähler, in *Scattering*, edited by R. Pike and P. Sabatier (Academic Press, New York, 2002).
[28] T. Keller, K. Habicht, H. Klann, M. Ohl, H. Schneider, and B. Keimer, Appl. Phys. A: Mater. Sci. Process. **74**, S332 (2002).
[29] M. Bleuel, F. Demmel, R. Gähler, R. Golub, K. Habicht, T. Keller, S. Klimko, I. Koeper, S. Longeville, and S. Prokudaylo, in *Neutron Spin Echo Spectroscopy*, edited by F. Mezei, C. Pappas, and T. Gutberlet, Lecture Notes in Physics Vol. 601 (Springer, New York, 2003).
[30] K. Habicht, T. Keller, and R. Golub, J. Appl. Crystallogr. **36**, 1307 (2003).
[31] T. Keller, K. Habicht and R. Golub, in *Neutron Spin Echo Spectroscopy*, edited by F. Mezei, C. Pappas, and T. Gutberlet, Lecture Notes in Physics Vol. 601 (Springer, New York, 2003).
[32] P. Vorderwisch, U. Stuhr, and S. Hautecler, J. Neutron Res. **7**, 119 (1999).
[33] M.J. Cooper and R. Nathans, Acta Crystallogr. **23**, 357 (1967).
[34] M.T. Rekveldt, R. Golub, and T. Keller, Europhys. Lett. **54**, 342 (2001).
[35] P. Vorderwisch, S. Hautecler, F. Mezei, and U. Stuhr, Physica B **213-214**, 866 (1995).
[36] A.A. Maradudin and V. Ambegaokar, Phys. Rev. **135**, A1071 (1964).
[37] S. Bose (private communication).
[38] R. Youngblood, Y. Noda, and G. Shirane, Solid State Commun. **27**, 1433 (1978).
[39] V.I. Bobrovskii, A.V. Goshchitskii, A.V. Mirmel'shtein, and Y.N. Mikhailov, Zh. Eksp. Teor. Fiz. **70**, 1820 (1976) [Sov. Phys. JETP **43**, 947 (1977)].